Supplementary Information

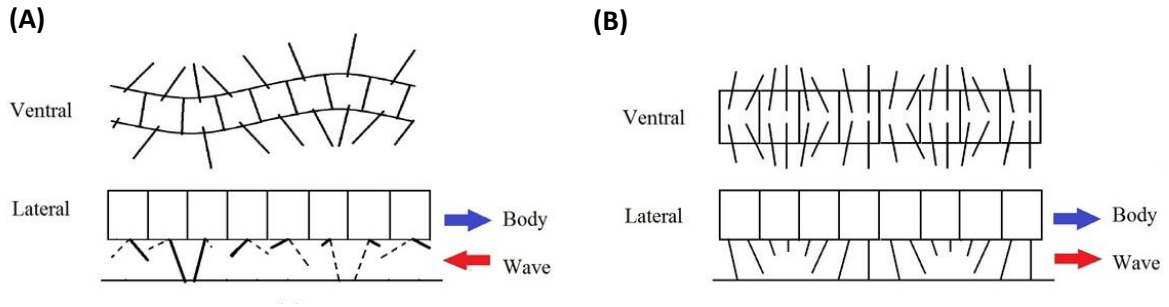

Figure S1: (A) Schematic of ventral and lateral view of a centipede gait, (B) Schematic of ventral and lateral view of a millipede gait

Figure S1 shows a comparison between the general gait patterns of the myriapod classes of the Chilopoda (centipede) and the Diplopoda (millipede). S1A shows the lateral undulating body with a metachronal gait exhibited by centipedes, maximizing stride length effective for high speed, where the effective traveling wave is opposite to the resulting body motion. Figure S1B shows the powerful metachronal gait used by millipedes, where the body does not exhibit extra undulations and the legs generate a traveling wave that moves in the same direction as the body motion.

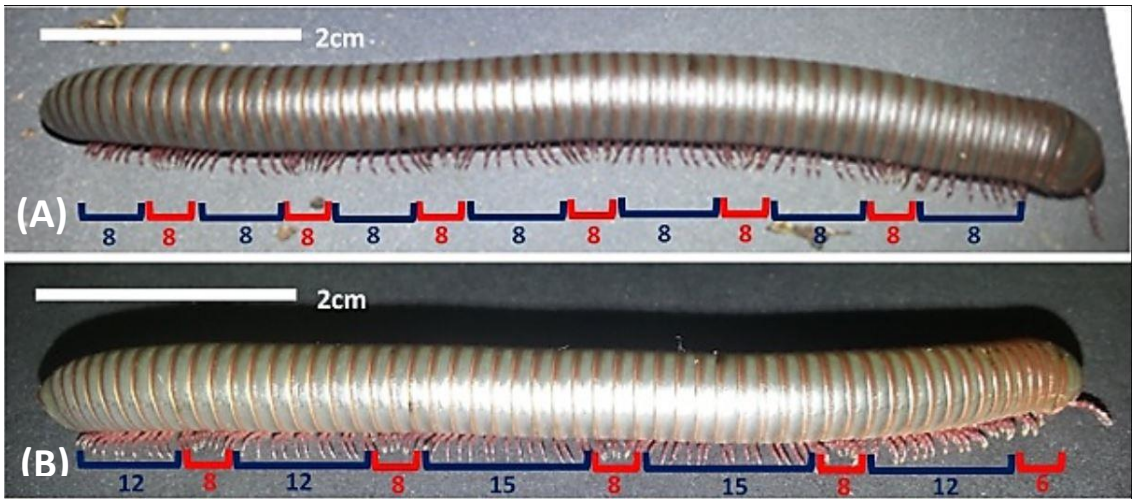

Figure S2: (A) Millipede walking gait with no resistance to motion (flat terrain). (B) Millipede walking gait with large resistance to motion (climbing sloped incline).

Figure S2 shows two cases in which a *N. americanus* millipede reveals the variation in their metachronal gait. Figure S2A is the specimen walking on a flat surface where a single traveling wavelength consists of a total of 16 legs. Here eight legs are in the propulsive backward stroke phase and eight legs are in the elevated forward stroke phase. When the environment is adjusted by increasing resistance against the direction of motion, by introducing an incline to the surface in Figure S1B, there is a clear adjustment in gait. Over a single wavelength, there are up to 27 legs per wave. While still there are eight legs in the elevated forward stroke phase, there are now up to 15 legs in the propulsive backward stroke phase.

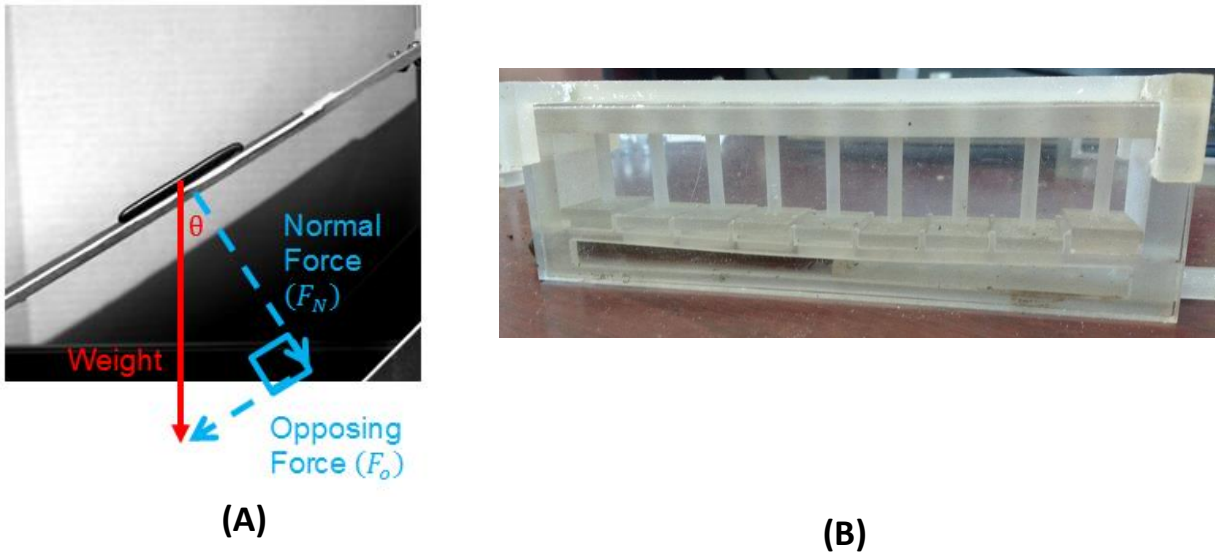

Figure S3: (A) Climbing incline slope experimental setup and depiction of forces, (B) Burrowing stage experimental platform

Figure S3 is a picture of a *N. americanus* climbing up the inclined slope platform. This experimental stage was home-built and driven by a stepper motor to ensure accuracy and repeatability of the randomly selected slope angles to have the millipede specimens climb. This schematic also indicates the forces of interest involved, that are needed to calculate the effective resistance force.

Figure S4 shows high resolution photographs of the legs for both species of millipedes used in this investigation, the *N. americanus* and *A. virginiensis*. The goal is to clearly show that they do not possess specialized features found in insects or arachnids that they can utilized to improve adhesion capabilities through techniques of van der Waals forces, capillary forces, or even small pincers to grasp.

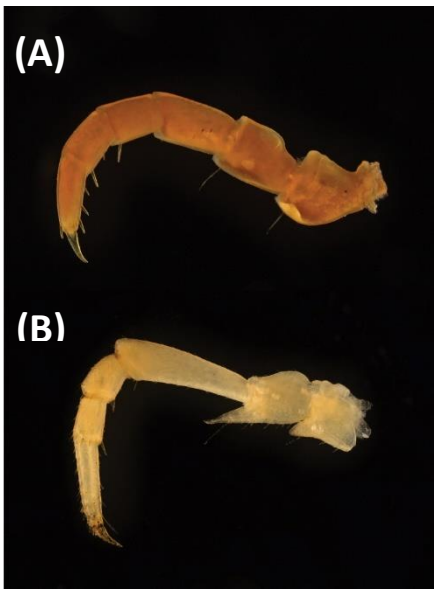

Figure S4: High resolution photographs of millipede species legs, which are without any specialized ends to assist with surface adhesion. (A) *N. americanus* Leg. (B) *A. virginiensis* Leg (Bottom)

(A)

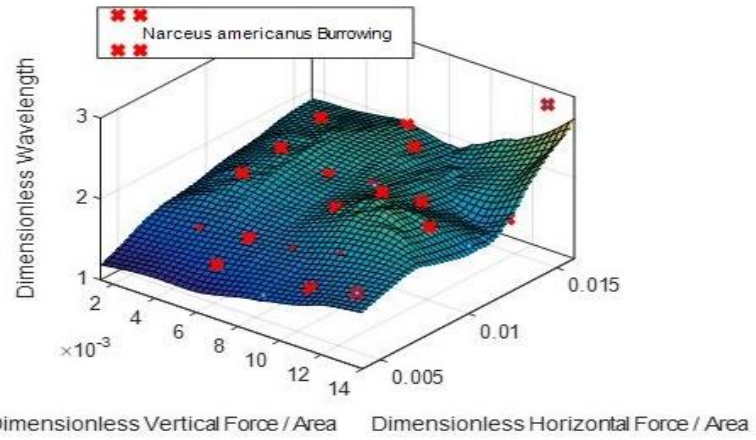

(B)

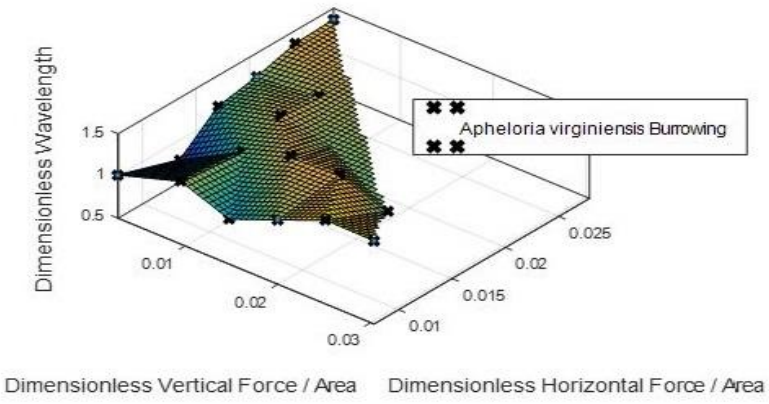

Figure S5: Surface plots of (A) *N. americanus* and (B) *A. virginiensis* dimensionless wavelength against horizontal and vertical load combinations per unit contact surface area.

Dynamic Modeling:

Equation S1-S4: Dynamic Modeling Approach

Static Analysis (Figure S6A):

$$\sum F_{STi} = 0 \qquad where\ for\ leg\ i\ F_{ST} = K\sin(\theta) \qquad (1)$$

$$\sum F_{SNi} = Weight \qquad where\ for\ leg\ i\ F_{SN} = K\cos(\theta) \qquad (2)$$

Propulsion Analysis (Figure S6B):

$$\sum F_{PTi} = F_R \qquad where\ for\ leg\ i\ F_{PT} = K\cos(\theta) \qquad (3)$$

$$\sum F_{PNi} = F_V \qquad where\ for\ leg\ i\ F_{PN} = K\sin(\theta)\ \text{*initial model}$$
$$where\ for\ leg\ i\ F_{PN} = K(\cos(\theta) - \sin(\theta))\ \text{*updated model} \qquad (4)$$

**Note K is a constant proportional to the segment weight and t is defined as seen in Figure S6E*

Dynamic Analysis (Figure S6C – initial model / Figure S8E – updated model): Static + Propulsion Forces

Equations S1-S4 are the set of equations used to determine the forces acting on the system. These equations correspond to the forces illustrated in Figure S6.

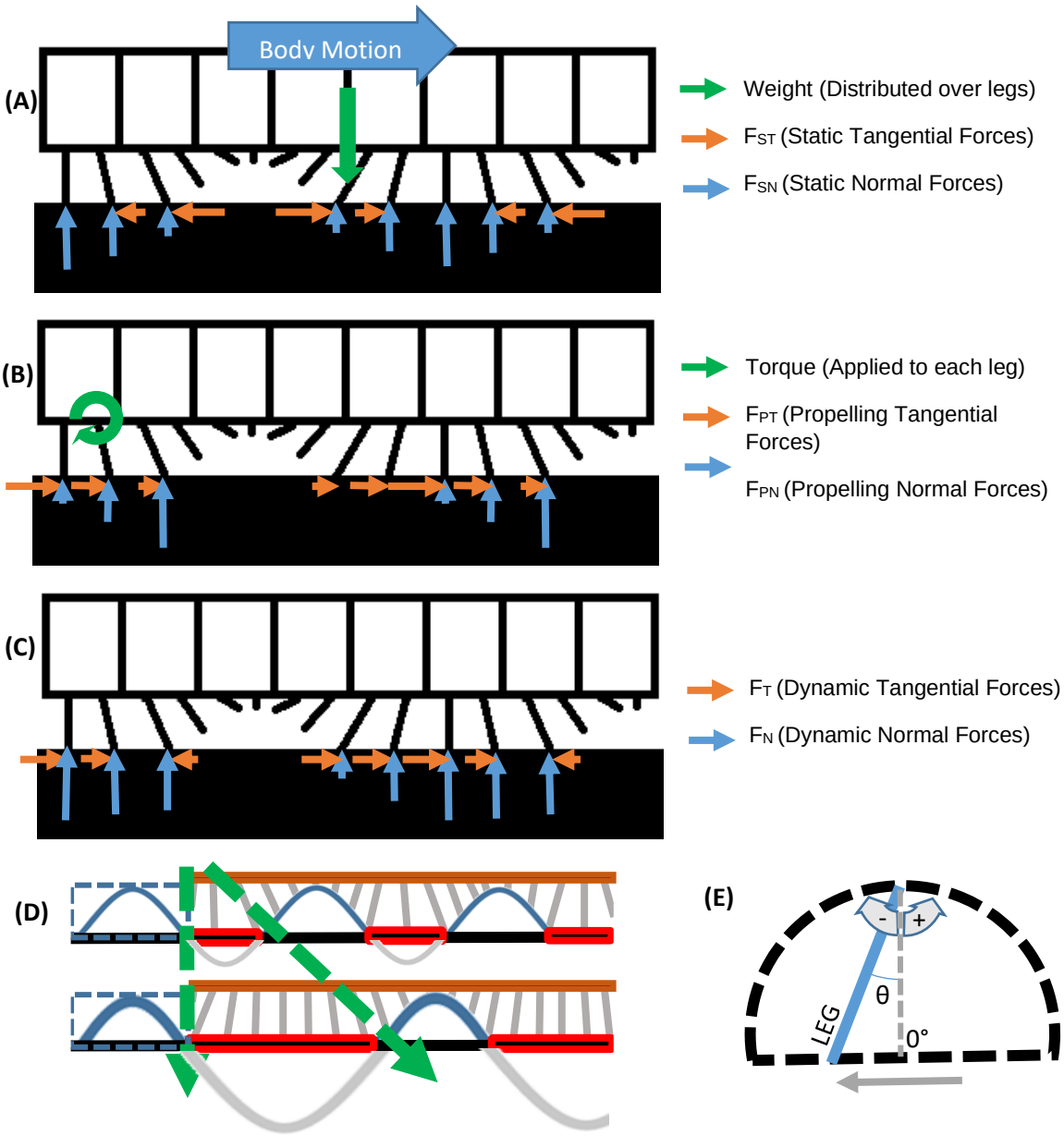

Figure S6: Schematic representation of the initial simulation model development. (A) Modeled ground reaction forces due to the static load distributed over millipede legs. (B) Forces generated due to applied torque motion at leg attachment point (single degree of freedom rotation at hip). (C) Resulting total Quasi-Static/Dynamic forces (summation of (A) and (B)). (D) Modulation in wave form to accomplish observed behavior (E) A schematic description of the angle θ used in Equations S1-4 and the orientation of the positive and negative directions.

Figure S6 schematically illustrates the ground reaction forces acting upon the legs of the millipede performing a metachronal gait. These diagrams show how the dynamic model was initially setup and governed, however adjustments were made to the ground reaction forces resulting from the torque applied by each leg. The changes made to Figure S6B to build a model consistent with experimental observations can be found in the main text, Figure 8D and 8E. Figures S6D illustrates how the modulation of a mechanically clipped wave increases the number of legs in contact with the ground. Figure S6E provides a visual reference of the angles used in the equations that govern the leg forces.

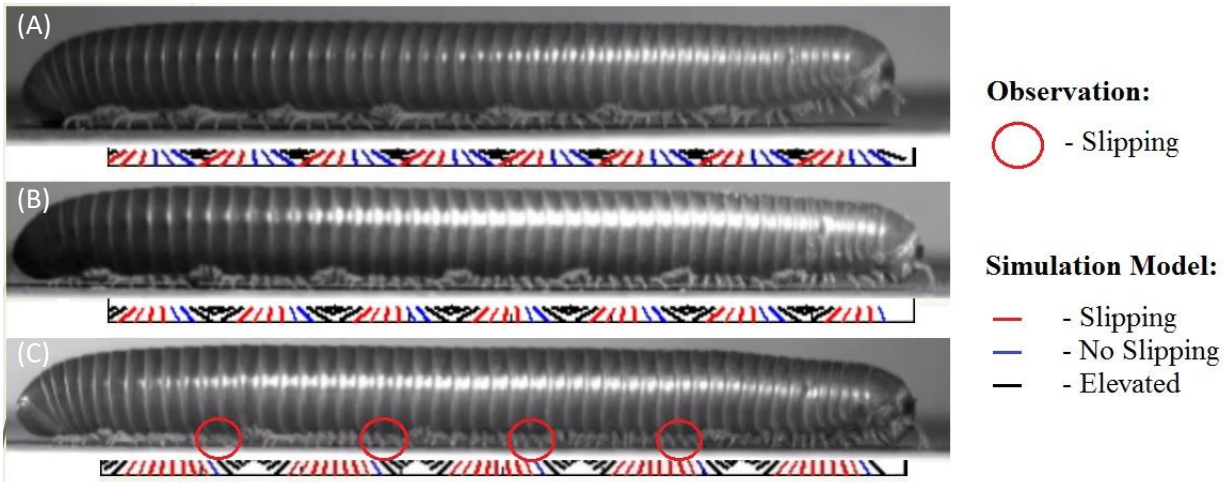

Figure S7: A comparison of locomotion experimental observation with initial dynamic model at different ramp inclines of (A) 5° (B) 30° and (C) 50°. Note this initial model uses the assumption of a single degree of freedom, which does not capture the observed slipping behavior of the legs.

Figure S7 compares the experimental observations with the initial dynamic modeling approach that assumed only a single degree of freedom for the individual legs. As shown, the observation of the actual millipedes (*N. americanus*) slipping only occurred at a large angle of 50° (Figure S7C). However, the initial modeling approach determined that slipping would occur in all cases, and even in the case where slipping actually did occur, the legs predicted to slip were inconsistent were contrary with actual behavior.

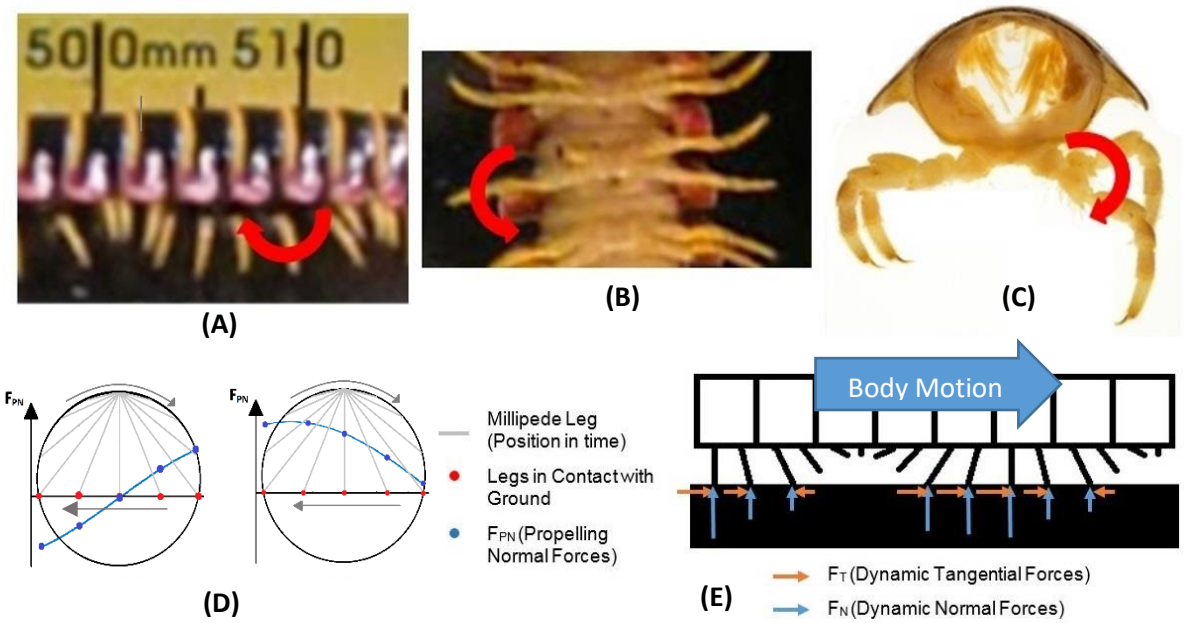

Figure S8: (a) Body line normal horizontal axis of rotation. (b) Vertical axis of rotation at hip joint for horizontal motion. (c) Horizontal axis of rotation at hip joint for vertical motion. (d) Comparison of single degree of freedom leg propulsive force model (left) with multiple degree of freedom propulsive force model (right). (e) Resulting leg force dynamics with updated model.

Figure S8 illustrates the adjustments made to the dynamic model to better capture the observed experimental motion. Figures S8A, B and C show the degrees of freedom observed in actual millipedes that were overlooked in the initial model. Figure S8D and E illustrate the force profiles that result from incorporating a level of control permitted by the extra degrees of freedom.

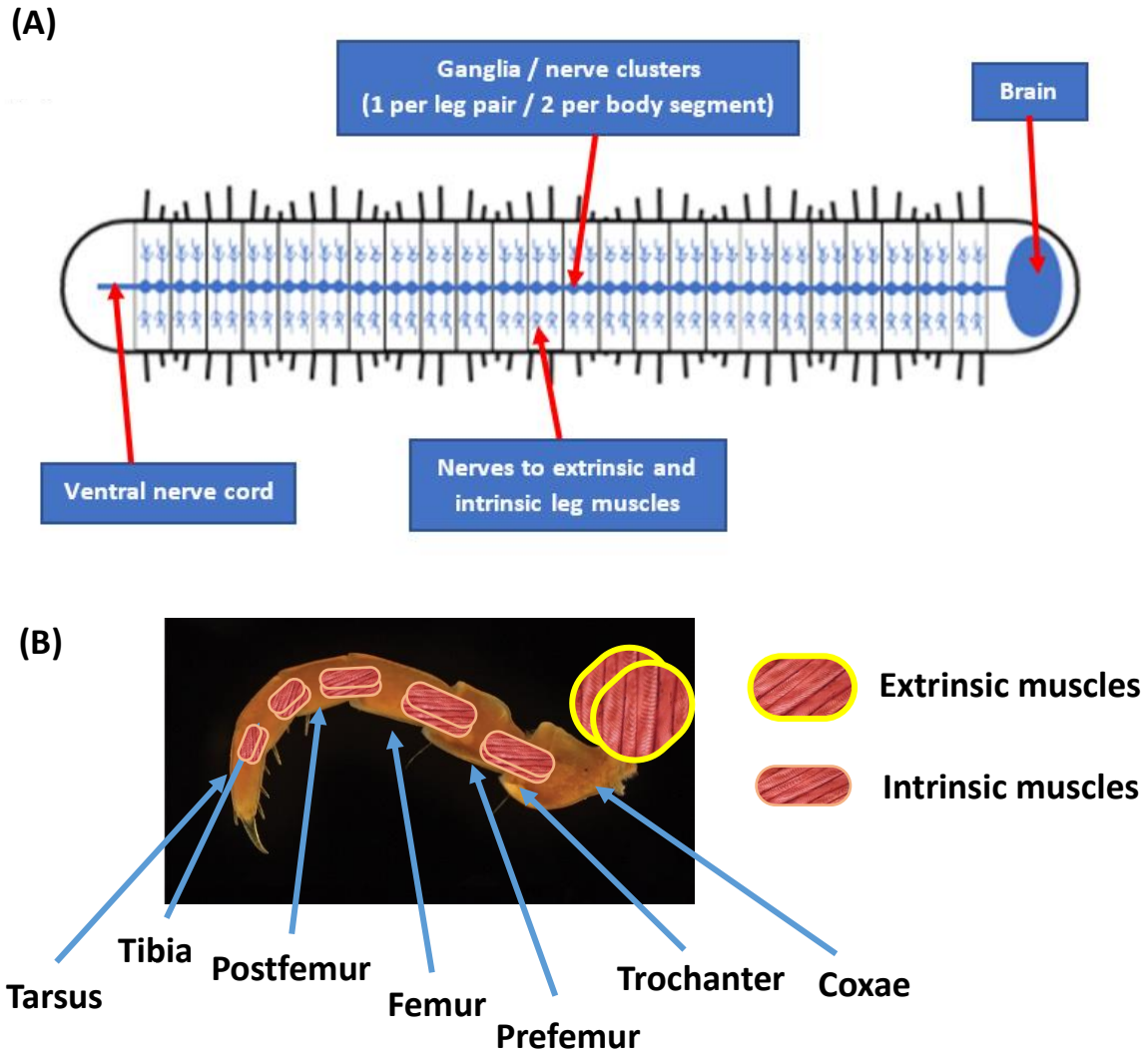

Figure S9: A generic glimpse of a millipede's anatomy utilized to accomplish control of independent legs. (A) Schematic of the Central Nervous System, (B) Schematic of the individual leg musculoskeletal structure

Figure S9 shows the maximum forward thrust performed by an individual leg for different cases of inclined slopes (thus resistance force) for the two species tested. For both cases, it revealed that the performance of an individual leg does not change drastically, indicating that the overall forward thrust is not dependent on the force output of an individual leg, but by modulating the effective traveling wave characteristics, aggregate behavior of all the legs combined is the main governing factor in increasing thrust.

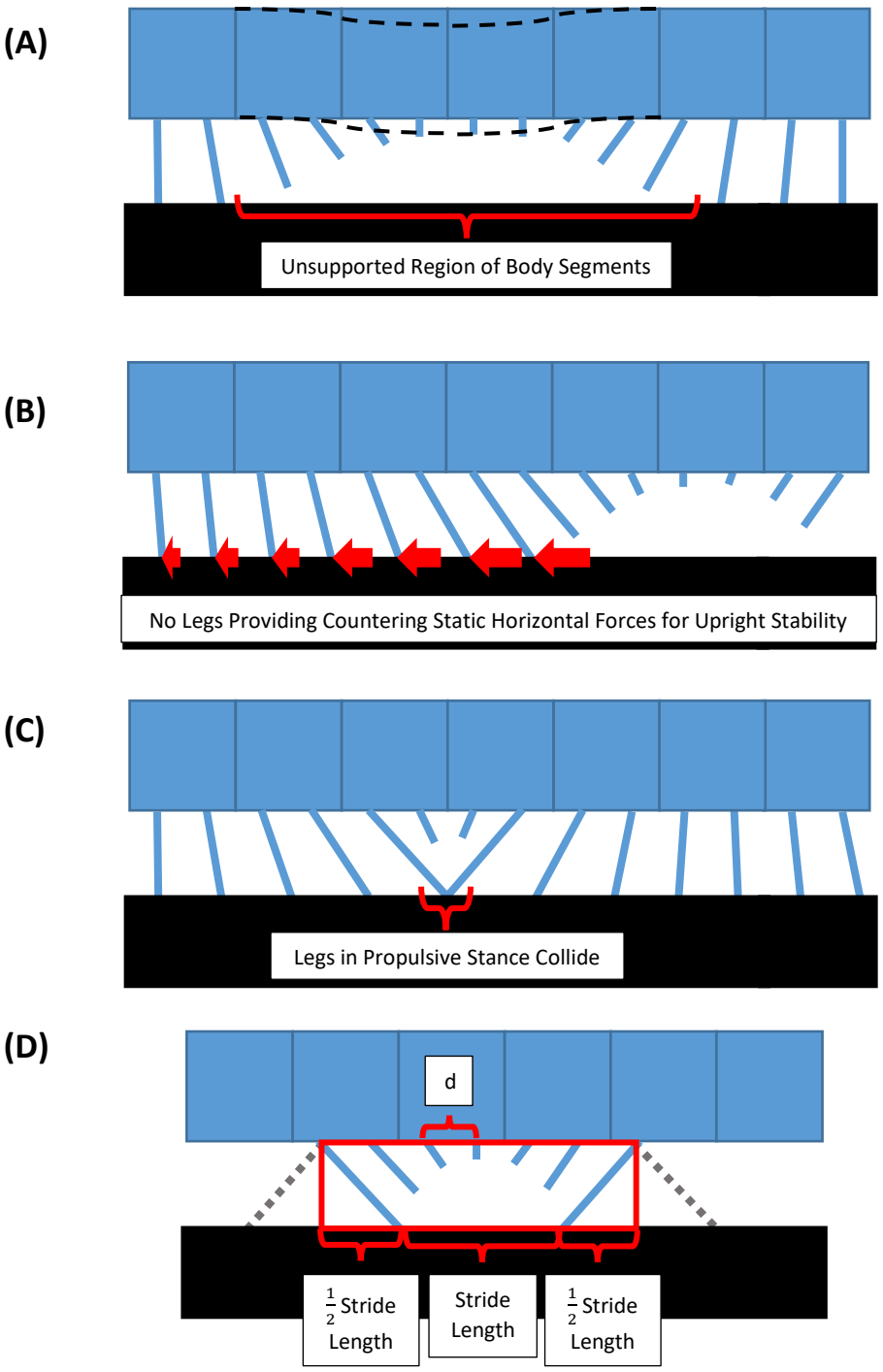

Figure S10: (A) Too many legs elevated per wavelength results in a large region of body segments without vertical support (B) Too long a wavelength (or too small a phase difference) results in upright instability (C) Too few legs elevated per wavelength could result in collision be legs in stance phase (D) Schematic of how legs elevated (temporal phase) is determined based on the morphological parameters

Figure S11 shows millipede robot leg mechanism inspired by the work of Wan et al. [32]. The mechanism is driven by a single DC motor at two different velocities using a PID control scheme. The two different velocities provide trajectories of the leg end effector performing a straight line (to propel body) and a circular arc (leg elevated from the ground). The mechanism was built using a combination of 3D printing and laser cutting.

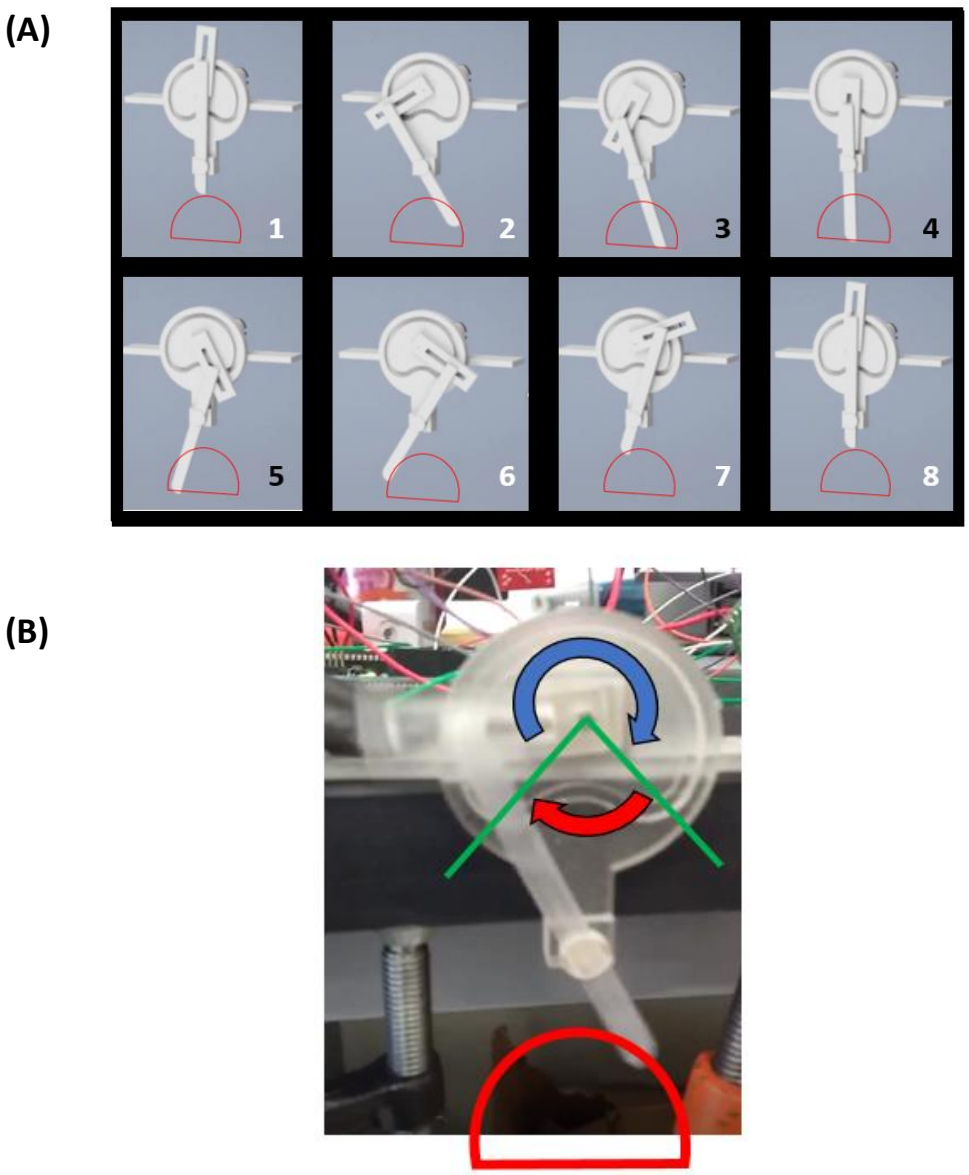

Figure S11: (A) Time frame instances of leg mechanism CAD simulation. Frame instances 3, 4, and 5 the leg is in contact with the ground performing a straight line motion. Frames 1, 2, 6, 7, and 8 the leg is elevated tracing a circular path, (B) Control scheme for individual leg motion: the two arrows indicate two different regions to define an angular velocity. The blue arrow indicates the region of the cam track that causes the leg to elevate, while the red arrow indicates the region where the angular velocity of the motor drives the linear motion of the leg

Figure S12 shows the millipede robot control scheme and physical structures. The structure was inspired by actual millipede biology seen in Figure S9A. The structure consists of a master and multiple slave segments. The master indicates the angular velocities in which the motors will operate as well as the phase difference between leg pairs. The slaves control an individual segment that drives the attached leg pairs.

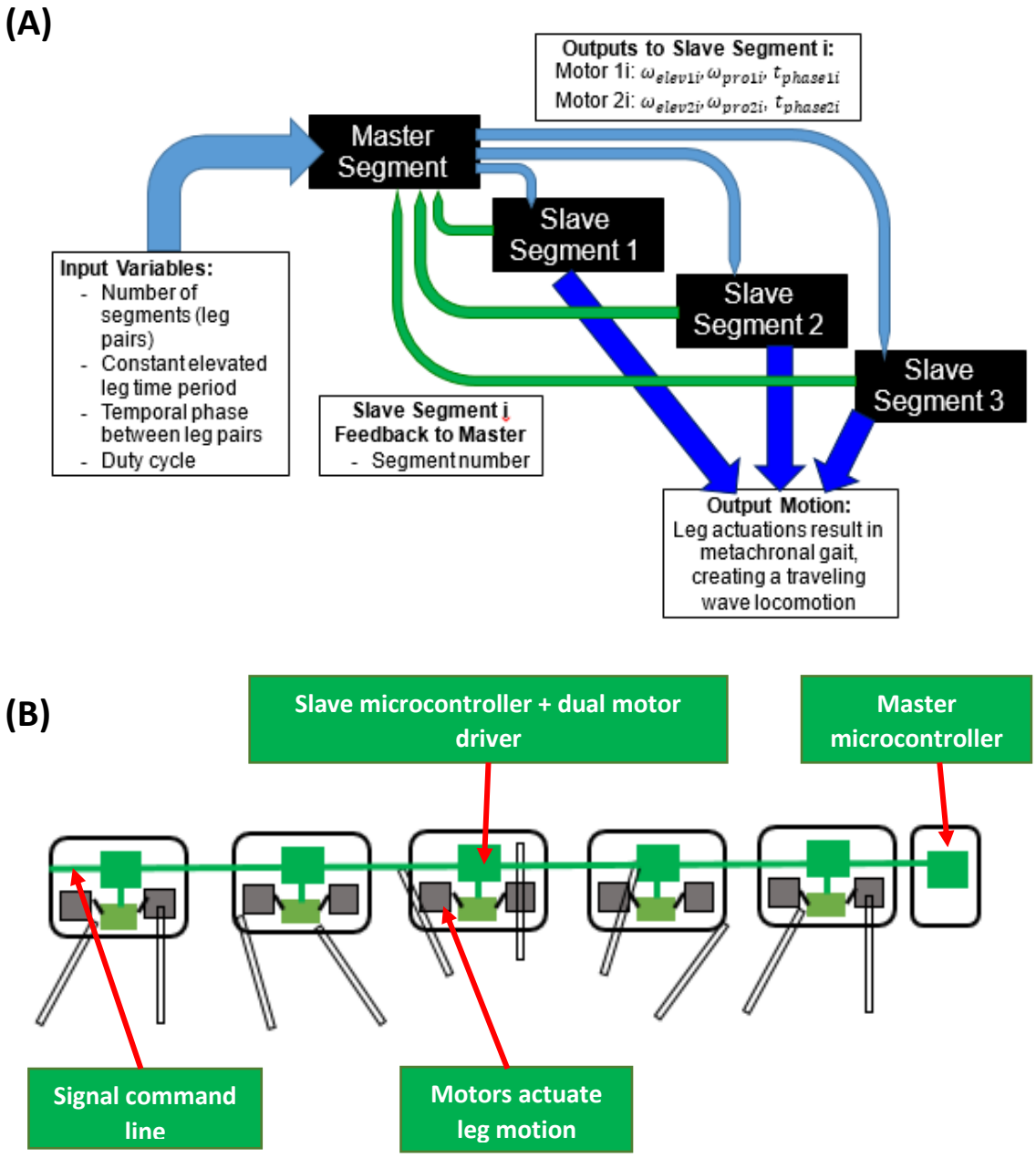

Figure S12: (A) Control scheme for bio-mimicking millipede robot to perform range of metachronal gaits (B) A visual representation of the electronics and control scheme of the proposed millipede robot design

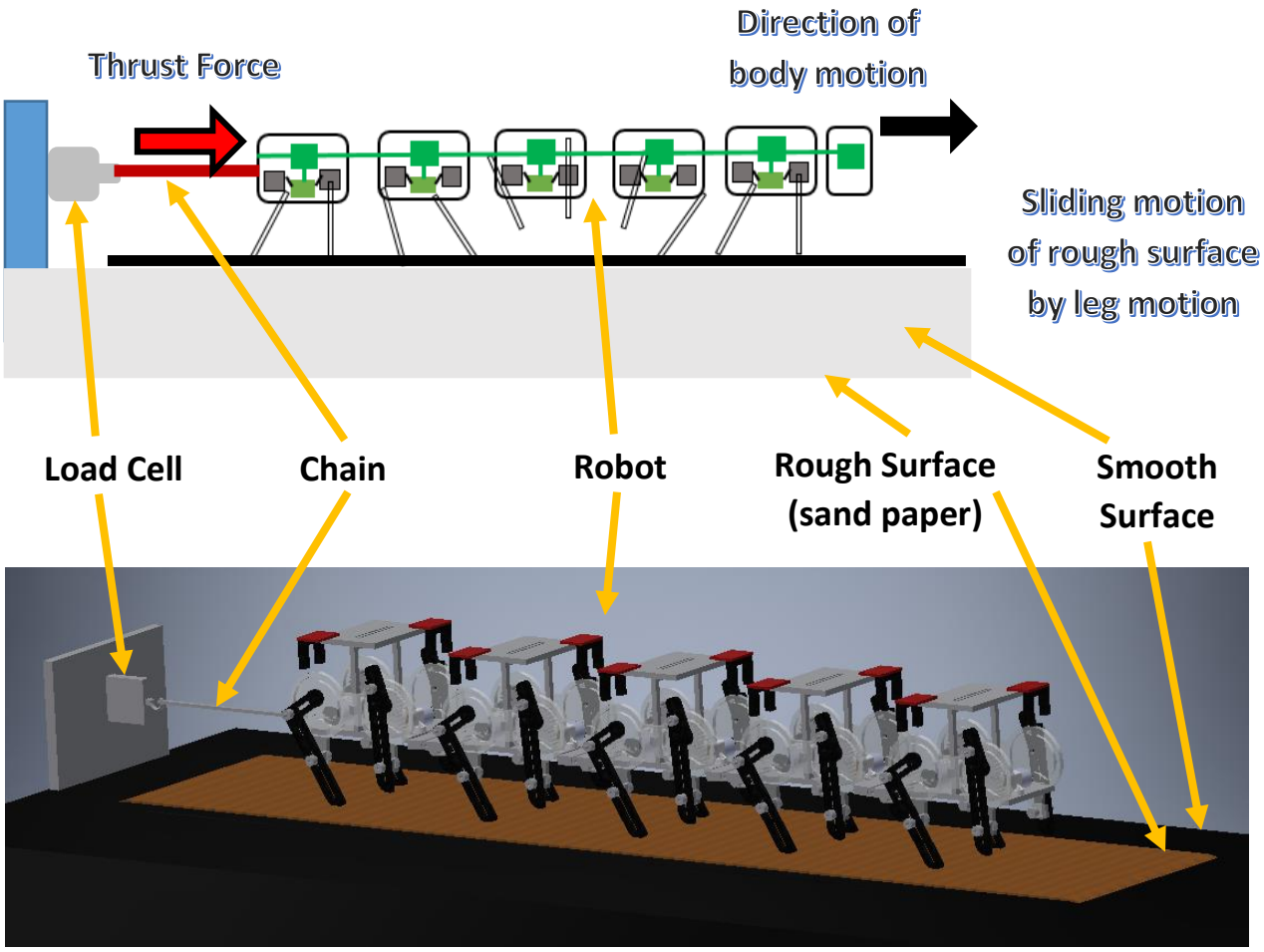

Figure S13: Experimental setup to determine the millipede robot locomotion thrust capabilities, measured directly from a load cell.

Figure S13 shows the experimental setup for the millipede robot. The robot platform walks on a rough surface (sand paper) that slides on a smooth acrylic surface, while the robot is attached by a chain to a fixed load cell. As a result, the locomotive thrust forces generated by the legs to propel the body forward are transmitted to and read by the load cell. This experiment was performed on the robot ranging from 1 to 5 body segments, exhibiting gaits of duty cycles, 0.3, 0.5, 0.7.

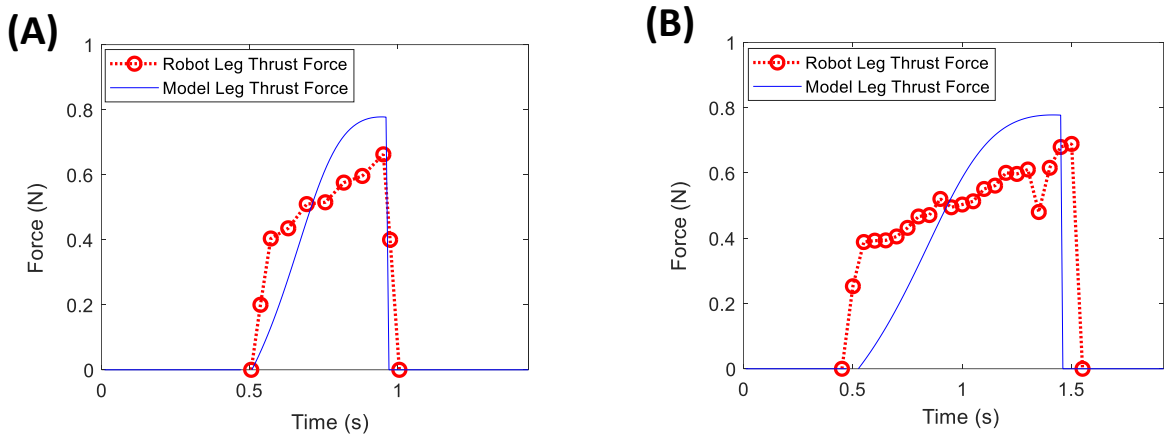

Figure S14: (A) Individual leg thrust force for a duty cycle of 0.33 (B) Individual robot leg thrust force for a duty cycle of 0.5

Experiment Specimens

Table S1 and Table S2 (*N. americanus* and *A.virginiensis* respectively) provide the dimensions of all the millipede specimens used in this investigation.

Table S1: *N. americanus* parameters

Narceus americanus					
Specimen	Body Length (cm)	Height (cm)	Width (cm)	Weight (g)	Number of Leg Pairs
1 (Climbing)	8.8	0.91	0.89	5.25	86
2 (Climbing)	8.4	0.91	0.77	3.91	91
3 (Climbing)	8.1	0.76	0.74	3.12	85
4 (Burrowing)	8.9	0.81	0.77	5.09	89
5 (Burrowing)	10.7	0.79	0.74	4.68	96
Model	10.0	0.8	0.8	5.00	90

Table S2: *A. virginiensis* parameters

Apheloria virginiensis					
Specimen	Body Length (cm)	Height (cm)	Width (cm)	Weight (g)	Number of Leg Pairs
1 (Climbing)	5.1	0.67	0.99	1.84	30
2 (Climbing)	5.4	0.61	0.99	1.51	30
3 (Climbing)	4.5	0.56	0.79	0.96	30
4 (Burrowing)	4.9	0.47	0.75	1.56	30
5 (Burrowing)	5.6	0.64	0.95	2.54	30
Model	5.0	0.6	0.8	2.00	30

Table S3: Kinematic equations and parameters

Circle Path Radius (R)	2-4.5mm
Elevation of leg height (H)	1.5mm
Stride	$2\sqrt{R^2 - H^2}$
Time transfer stage/forward stroke (T_T)	0.5
θ	$2\cos^{-1}(1 - \frac{H}{R})$
ω	θ/T_T
Wave Velocity	ωR
Time propel stage/backward stroke (T_P)	$T_T(Duty\ Cycle)/(1 - Duty\ Cycle)$
Body Velocity	Stride/T_P

Table S4: Robot segment parameters

Robot Segment Morphological Parameters	
Weight	1.2N
Diameter	0.05m
Length	0.09m
Leg Spacing (d)	0.047m
Stride Length	0.04m

Video S1 – Narceus americanus walking on 25° incline

Video S2 – Narceus americanus walking inside burrowing stage

Video S3 – Millipede robot

Video S4 – Narceus americanus simulation model with duty cycle of 0.3

Video S5 – Narceus americanus simulation model with duty cycle of 0.7